Porous media description using 3D non-uniform generalized cylinders and computed tomography images

Ndeye Fatou Ngom, Cheikh H.T.Cherif Ndiaye, and Oumar Niang

Abstract— In this paper, computer Tomographic techniques is used to study complex porous media in three dimensions. A methodology for extracting topologically equivalent networks of porous media from soil images samples is presented. The proposed description approximates the pore space using non-uniform generalized cylinders. We show that the non-uniform generalized cylinders matches more the real soil pore galleries than other primitives such as uniform generalized cylinders. Formula to compute quantitative characteristics on the generalized cylinder like length, tortuosity, volume and soil properties characteristics such as hydraulic conductivity are also proposed. New concepts (degree of compactness and variability) are used to compare the different representations. The description is applied to real soil 3D CT images and the results are compared to a previous published paper based on the same data. The tools we used enabled us to have a more autonomous and dynamic computation.

Index Terms— 3D reconstruction, Computed tomography images, Pore network, Porous media, generalized cylinders.

1 Introduction

Recent advances in imaging technologies have been used to obtain accurate 3D characterizations of complex pore space geometry, to visualize and quantify pore structural changes [13,19,23]. The availability of microscopic scale data, combined with the anticipation of further advances in the very near future in terms of both laser and X-ray technologies opening up even brighter prospect, has prompted researchers to develop an array of sophisticated models at the pore scale [17]. However the results of image based modeling studies depend crucially on the employed model and the quality of the pore space image on which the model runs [13]. Given the complexity and the heterogeneity of natural porous media, non-destructive characterization techniques such as X-ray computed tomography techniques (X-ray CT) are more suited to extract structural information of the porous material in the physical three dimensional space and quantify pore structural changes through a simplified version of the complex void space referred to pore network [4,24,3].

Pore network consist of an interconnected network of pores (or nodes) and throats (or bonds) and have been widely used in porous media modeling to study flow, transport phenomenon, organic matter decomposition and microbial dynamic [14,8,9,22,11]. The manner in which pores are connected to their nearest neighbors constitutes the network topology while the specific geometric idealizations used to represent pores and throats define the network geometry [25]. Thus the most critical step prior to any modeling effort is the accurate characterization of the pore space geometry and topology. To ensure the preservation of topological structure of the solid void interface, skeleton is a search path of a good characterization of pore by set of geometric primitives. In the cases where theses primitives are balls, the center of maximal balls obtained through Delaunay triangulation of the soil structure shape is often used to generate the skeleton [21,16,19]. However, as a maximal ball can be including in the set of maximal balls representing the pore space, their number can be reduced.

To ensure the conservation of topological properties while performing the minimization process, the concept of pore space hierarchical representation was introduced [13,14]. The pore space is first decomposed by a minimal set of balls covering the skeleton. Then by connected chains of balls which is afterward used to represent pore channel by primitives such as cylinders and circular

generalized cylinders.

However there were some limitations: loss of volume during the approximation process, no variation of pore channel radius and no possibility of network deployment. To overcome these limitations, in the present study, the uniform generalized cylinders concept is extended to the non-uniform case to provide a more accurate approximation of pore channels.

A non-uniform generalized cylinder is a generalized cylinder whose distance between its skeleton and its boudaries is not constant along its length.

Fig.1 Schematic diagram of the processing steps

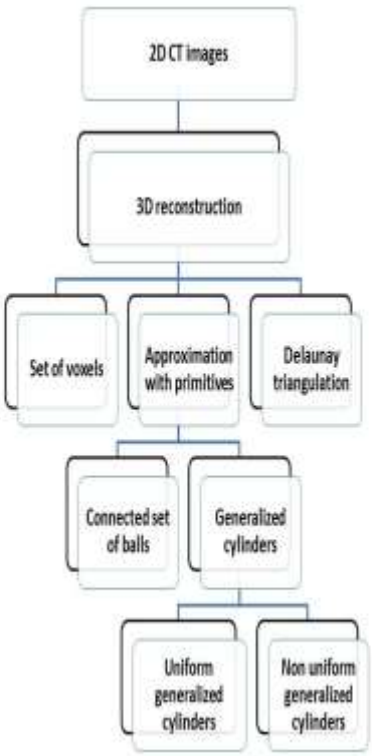

The proposed non-uniform generalized cylinders matches more real soil pore galleries than the uniform generalized cylinders and can be used in the analyze of soil burrow systems [15,18]. We also provide formulas to compute some porous media quantitative characteristics from this description and give some illustrations with real soil data. To have an autonomous and continuous platform computation and thus minimize the approximation errors, the Java language and its associate libraries were used to implement the computation steps on one platform.

Section 2 gives an overview of the pore space extraction process from computed tomography images. The proposed approximation and the images acquisition images process are discussed. Section 3 introduces the pore channels description with balls and the extraction procedures. Section 4 presents the pore channels representation with generalized cylinder. Section 5 gives formulas and illustrations for the computation of quantitative characteristics such as length, tortuosity, volume, porosity and saturated hydraulic conductivity. Section 6 is about the pros and cons of the uniform and non uniform generalized cylinders representation.

2 3D Description of Microstructures

2.1 Pore space extraction

From a set of 2D computed tomography images (Fig.1, Fig.2), volume description is extracted by a straightforward superposition process along the same *axes followed by sampling constraints. The height of each* voxel is the distance between two CT images along the axes. Thus, the primary volume description is a set of voxels. The pore space is obtained from thresholding. The result is a tridimensional binary image. The binary representation allows distinguishing the pore space from the core space of the soil volume. The boundary points are the points having at least one neighbor that does not belong to the pore space. The set of boundary points is extracted in three dimensions using the 26-connectivity and represent less than 10 % of the pore space voxels [10]. Having the boundary of the pore space, the next step is to approximate the volume of the pore space by primitives that can be used for example to simulate organic matter decomposition or fluid transfer inside the pore space. Ngom et al [13,14] calculates a minimal set of maximal balls that recover the skeleton of the pore space using Delaunay tessalation [6,7].

This primary description ensures the conservation of topological properties but the approximation by balls involves a loss in volume. Thus the set of balls were segmented on simply connected sets that is considered as pore channels that is afterward approximated by cylinders or uniform generalized cylinders. However there were some limitations such as lost of volume. Indeed the uniform approximation process does not take into accounts local variation of pore channel radius and thus can lead to a shape different from the initial shape. To overcome these limitations, in the present study, the uniform generalized cylinders concept is extended to the non-uniform case to provide a more accurate approximation of pore channel.

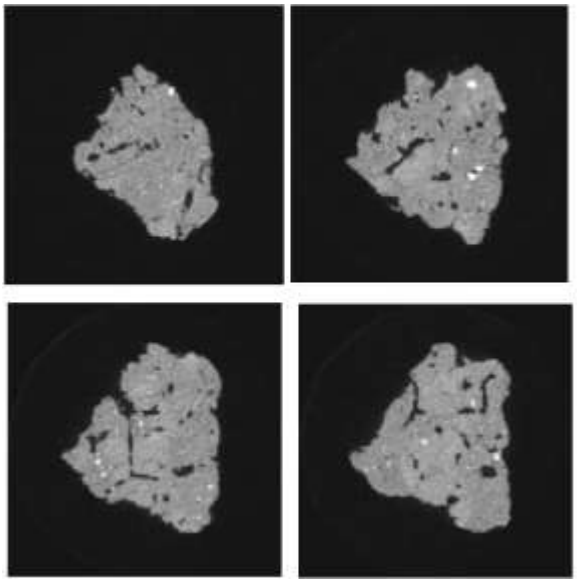

Fig.2 Example of four sections of two dimensional CT images

2.2 The Proposed Model

A non-uniform generalized cylinder is a generalized cylinder whose distance between its skeleton and its boundaries is not constant along its length. This description gives realistic representation of pore channel that can save much computing time and memory space during simulation inside soil or rock aggregates and can be helpful when looking for global characteristics of pore space for classification purposes. It provides continuous and rounded shaped pores which are interconnected with each other via lateral pores. It can also be used in the analyze of soil burrow systems such as biopores influenced either by deep rooting taproots or earthworms in natural conditions [15,18].

In this work, a unique platform is used for the implementation to straighten the successive approximation process and to have a good control of all the transform steps. In the previous studies [13,14] the used language (C) presented some limitations for networked deployment and the two different platforms used during the processing steps did not allow to perform dynamic autonomous simulation. In the present study, the program has been written in Java and thus can be easily transferred in Java Applet, so it can run in the internet. The real time rendering of the model require 3D toolbox such as Java3D and JOGL to set up the 3D virtual universe [5]. In the whole process, we can at the same time compute the approximation and visualize the results on a single window with different viewpoints.

2.3 Images acquisition and description

To illustrate the proposed description, a computed tomography (CT) images soil sample obtained by Peth et al [16] from soil aggregates using synchrotron X-ray is used. The soil has the following texture: 10% sand 70% silt and 20% clay. The soil data have been sampled at the experimental research farm Rothamünster southern Germany from an unplowed horizon which has been under grassland use since 1961. The soil was scanned at the synchrotron radiation for x-ray microtomography SR-µCT (at DESY, Deutsches Elektronen Synchrotron in Hamburg Germany). The resolution was 5.403 µm with a dimension of 400x 400x400 voxel sized cube.

A perspective view of the set of images samples is presented in Fig 2. Fig 3 shows examples of CT images before and after thresholding. Fig 4 gives an example of volume representation computed from 100 CT images after thresholding.

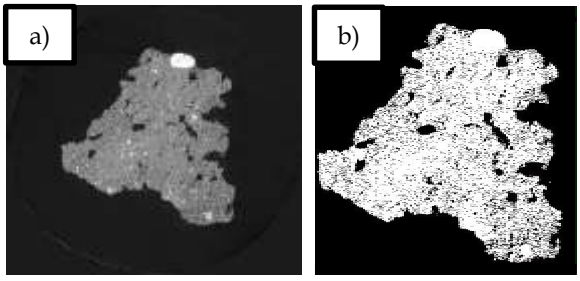

Fig.3 Extraction of contours points by thresholding: a) gray CT image, b) binary CT image.

(a) 3D soil structure after reconstruction of 100 two a.

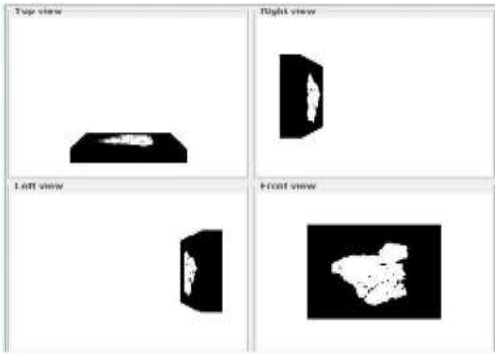

(a) dimensional CT images

(b) 3D pore soils voxels after thresholding of segment of 3D volume

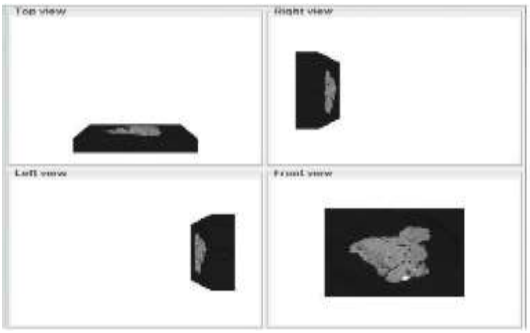

Fig.4 Four different views of the 3D structures

3 Pore channel Extraction

3.1 Description of pores with balls

From the Delaunay triangulation, balls description of pore space is easily generated as a set of Delaunay spheres. A Delaunay sphere attached to a tetrahedron is the sphere passing through the four vertices of the tetrahedron. The approximation of volume shape by balls is obtained by computing for each tetrahedron its circumscribed spheres. And all the centers of Delaunay spheres included within the shape gives the skeleton [4] which is often called medial axes. From this step we obtained a set of disjoint or tangent maximal balls describing shape cavities. Fig 5 gives perspectives views of the balls description of pore structures with 4000 balls and 50000 balls.

3.2 Pores channels extraction

We suppose that the pore channel is formed by simply connected balls. A connected set of balls is a pore channel if and only if [14]:

1. Each ball of the chain is connected to more than two balls in the chain,
2. Two balls of the chain are connected with only one other ball in the chain.
3. For each ball in the chain that was connected to two different balls in the chain, if the ball is removed from the chain then the chain will be split in two connected components, a chain could be built with at least two balls.

4 Non-uniform generalized cylinders Approximation

The balls representation is a primary representation of the pore channels. However, the generated shapes are far from the reality where we have to deal with galleries. Thus to strengthen this description, the ball description of each pore channel is approximated with generalized cylinders. We first approximate the center of the balls describing the pore channel with a Hermite spline. Then we generate a revolution surface.

Fig.5 Perspectives views of pore space and pore channels description with balls: a) 4000 balls b) 50000 balls c) set of of pore channels

Fig 5(c) gives examples of pore channels computed from the balls description of Fig 5(b).

Fig.6 presents the processing steps during the computation of the generalized cylinder. As illustrated, the skeleton of the ball chain is first computed from a simply connected set of balls. Then, a uniform generalized cylinders or a non-uniform generalized cylinder is generated from the skeleton taking into account the radius of the balls.

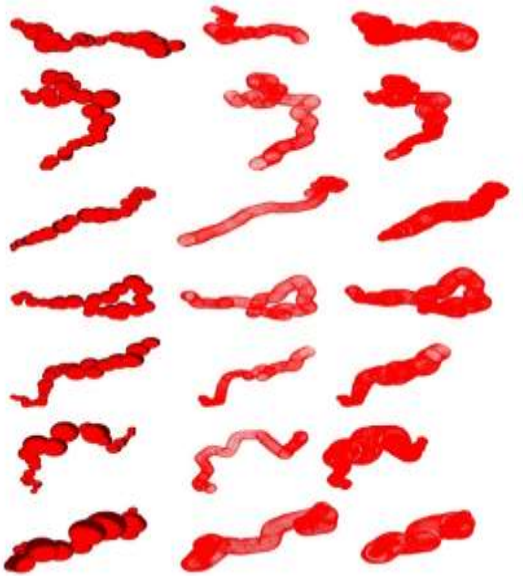

4.1 Generalized cylinder

There are many definitions of a generalized cylinder. But for computations purposes, a definition based on controls points is preferred [5,20]. A generalized cylinder is described parametrically as follows

$$Ps\,(t) \;=\; [pos\,(t), rad] \qquad (1)$$

Where *post (t)* is a piecewise cubic spline using a series of controls points *{P0, P1,..., Pn−1}* and rad refers to the distance between the spline and the contours of the spline. In this paper, the control points are the centers of balls, *rad* is a set of numerical values computed from the radius of the corresponding balls of the spline and *post(t)* is a parametric curve in 3D expressed as follows

$$pos(t) \;=\; (x\,(t), y\,(t), z(t)), 0 \;\leq\; t \;\leq\; 1 \qquad (2)$$

And

$$\begin{aligned} x(t) &= a0x + a1xt + a2xt^2 + a3xt^3 \\ y(t) &= a0y + a1yt + a2yt^2 + a3yt^3 \\ z(t) &= a0z + a1zt + a2zt^2 + a3zt^3 \end{aligned} \qquad (3)$$

x(t), y(t) and *z(t)* are in the same form but independent of each other except at drawing where they are used together to specify a point. We discuss in the following in the place of *x (t), y(t)* and *z (t)* the parametric function *p (t)* defined as follow

$$p(t) = at^3 + bt^2 + ct + g \qquad \text{Where } 0 \leq t \leq 1$$

4.2 The spline generation

To obtain a reasonable degree of continuity and flexibility that can be generated and evaluated efficiently, we choose to work with the Hermit spline [2]. The Hermit curves are specified by two end points *p (0)* and p (1)) and two tangent vectors (*p′ (0)* and *p′ (1))* at the two end points. The equation for a Hermit curve is

$$\begin{aligned} p(t) = (2t^3 - 3t^2 + 1)p(0) + (-2t^3 + 3t^2)p(1) \\ + (t^3 - 2t^2 + t)p'(0) + (t^3 - t^2)p'(1) \end{aligned}$$

which is expresses in the matrix form as follow

$$p(t) = (t^3 t^2 t\ 1) \begin{bmatrix} 2 & -2 & 1 & 1 \\ -3 & 3 & -2 & -1 \\ 0 & 0 & 1 & 0 \\ 1 & 0 & 0 & 0 \end{bmatrix} \begin{bmatrix} p\,(0) \\ p\,(1) \\ p'\,(0) \\ p'\,(1) \end{bmatrix} \qquad (5)$$

In our model p (0) and p (1) are the coordinates of two adjacent control points Pi and Pi+1. The tangents to the end points p′ (0) and p ′(1) are respectively Pi+1−Pi and Pi+2−Pi. Thus

$$p(t) = (t^3 t^2 t\ 1) \begin{bmatrix} 2 & -2 & 1 & 1 \\ -3 & 3 & -2 & -1 \\ 0 & 0 & 1 & 0 \\ 1 & 0 & 0 & 0 \end{bmatrix} \begin{bmatrix} Pi \\ Pi{+}1 \\ Pi{+}1 - Pi \\ Pi{+}2 - Pi{+}1 \end{bmatrix} \qquad (6)$$

Fig.6 Generalized cylinder: a) connected chain of balls, b) spline computed from the center of the balls, c) uniform generalized cylinder , d) non-uniform generalized cylinder

4.3 Uniform Generalized Cylinder (UGC)

A generalized cylinder with constant distant between the spline and the contours points is called uniform generalized cylinder [14]. The latter distance is called the radius of the uniform generalized cylinder.

The parametric function of equation 1 used to describe the UGC becomes

$$Ps(t) = [pos(t), rad] \qquad (7)$$

Where *rad* is the maximal balls mean radius.

The generation of the surface is done easily with a circle function c (u) according to *post (t)* to generate the surface of the uniform circular generalized cylinder. The uniform generalized cylinder is a straightforward way to approximate connected set of balls with 3D tubular shape. However sensibility to extreme values of the radius of balls is one of the main disadvantages. Indeed, little or great values of a radius in a chain of balls can greatly change the volume of the CGU computed from the ball chain as illustrated in Fig.6. Thus, to overcome this drawback, we defined the notion of non-uniform generalized cylinder.

6.1 Non Uniform Generalized Cylinder (NUGC)

If the distance between the skeleton and the contour points of the generalized cylinder is not constant, then we call it a non-uniform generalized cylinder. The parametric equation 1 become in this case

$$Ps(t) = [pos\ (t), rad] \qquad (8)$$

where *rad* is a set of local radius.

The choice of rad should be done efficiently to avoid continuity issues during the NUGC generation. Indeed, arbitrary radius will lead to subset of generalized cylinders like the one illustrated in Fig 8.

Let $B = \{B_1, \ldots, B_n\}$ the associated balls of a set of control points $P = \{P_1, \ldots, P_n\}$. The set of NUGC local radius $rad = \{r_1, \ldots, r_n\}$ is defined as follow

$$rad_i = \begin{cases} r_i & \text{If I} \in \{1, n\} \\ r_{i-1} + r_i + r_{i+1} / 3 & \text{If I} \in \{2, \ldots, n-1\} \end{cases} \qquad (9)$$

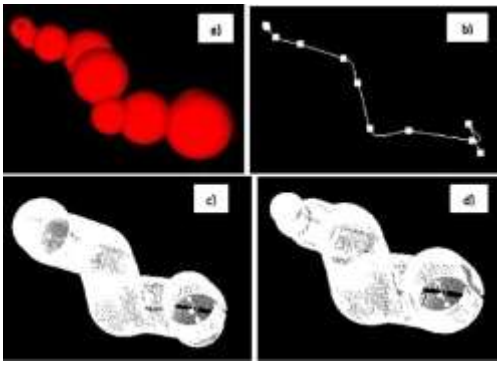

Fig.7 Uniform and non-uniform generalized cylinders computed from connected set of balls

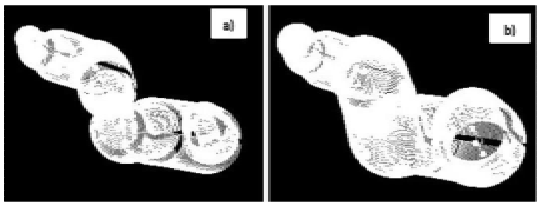

Fig.8 Continuity for CGUN generation: a) discontinuities on the boundary after computation b) continuity on the boundary

One of the advantages of defining local radius by equation 9 is the preservation of local topological and geometrical characteristics of pore channels. As illustrated in Fig 6, the non-uniform generalized cylinders matches more porous channel, than the uniform generalized cylinders. In the sequel, we provide way to compute some quantitative characteristics from the non-uniform generalized cylinders representation.

5 Quantitative Characteristics Computation on the GC

In [14], there were no clues on how to compute the length or the volume of a generalized cylinder. However, this is essential when we want to run simulation of physical process inside the approximated shape. Thus, in the following, formulas to compute quantitative characteristics are proposed and illustrated in the uniform case and in the non-uniform case. The length is the same for the two cases, but the volume varies according to the uniform generalized cylinder or non-uniform generalized description. Thus to simplify the notation, we will refer to UGC when the computed characteristics are the same for the uniform generalized cylinders and non-uniform generalized cylinders.

5.1 Length computing

Let's us suppose that we computed a generalized cylinder from n balls. The associated generalized spline has been extracted from n control points (centers of the balls) *{P0, ..., Pn−1}*. Let P_iP_j be the length along the spline between two control points *Pi* and *Pj*. Then by construction of pos_i(t)

$$P_iP_{i+1} = \| \int pos_i dt \| \qquad (10)$$

Thus

$$l = P_0P_{n-1} = \sum \left| \int pos_i(t) dt \right| \qquad (11)$$

From equation 6, we have

$$\int pos_i(t)dt = P_i \int (2t^3 - 3t^2 + 1)dt + P_{i+1} \int (-2t^3 + 3t^2)dt + (P_{i+1} - p_i) \int (t^3 - 2t^2 + t)dt + (P_{i+2} -$$

$P_{i+1}) \int(t^3 - t^2)$

It follows that

$$\int pos_i(t)dt = \frac{1}{12}P_i + \frac{1}{12}P_{i+1} + \frac{1}{12}(P_{i+1} - P_i) + \frac{1}{12}(P_{i+2} - P_{i+1})$$

Thus

$$\int pos_i(t)dt = \frac{5}{12}P_i + \frac{8}{12}P_{i+1} + \frac{1}{12}P_{i+2} \quad (12)$$

Finally, from equation 11 we have

$$l = \sum \left\| \int \frac{5}{12}P_i + \frac{8}{12}P_{i+1} + \frac{1}{12}P_{i+2} \right\| \quad (13)$$

The length gives insight on some key characteristics like tortuosity of the pore galleries.

5.2 Volume computing

1) *Uniform case*: In the uniform case, the UGC radius is defined as the mean of its associated balls. Thus, the UGC volume can be computed using the following formula

$$V = ||l * S|| \quad (14)$$

Where l is the length of its skeleton which is here a spline computed from the center of its associated balls and $V = 2\pi r$ where r is the main of the chain balls radius. From equation 13 it follows

$$V = S \sum_{i=0}^{n-1} \left\| \int \frac{5}{12}P_i + \frac{8}{12}P_{i+1} + \frac{1}{12}P_{i+2} \right\| \quad (15)$$

Fig 8 (a) gives a comparison of volume computed with the proposed CGU based model and the one computed from the corresponding set of balls. As illustrated, the shape of the two curves is the same even if higher volume is noted with the uniform generalized cylinder approximation. This is the consequence of the fact that we recover part of information that was lost during the chain balls approximation from the voxel representation.

2) *Non Uniform case*: In the non-uniform case, the generalized cylinder has local radius given by equation 9. The UGC volume can be computed using the following formula

$$V = \sum_i ||l_i * S_i|| \quad (16)$$

Where Si is the local surface of the corresponding circle with radius the local radius given by equation 9 and li is the length between two controls points defined as follow

$$l_i = P_iP_{i+1} = \int_0^1 pos_i(t)dt \quad (17)$$

It follows then from equation 17, that

$$V = \sum_i S_i \left\| \int_0^1 pos_i(t)dt \right\| \quad (18)$$

From equation 13, we have

$$V = \sum_i S_i ||l_i|| \quad (19)$$

Where

$$l_i = \frac{5}{12}P_i + \frac{8}{12}P_{i+1} - \frac{1}{12}P_{i+2}$$

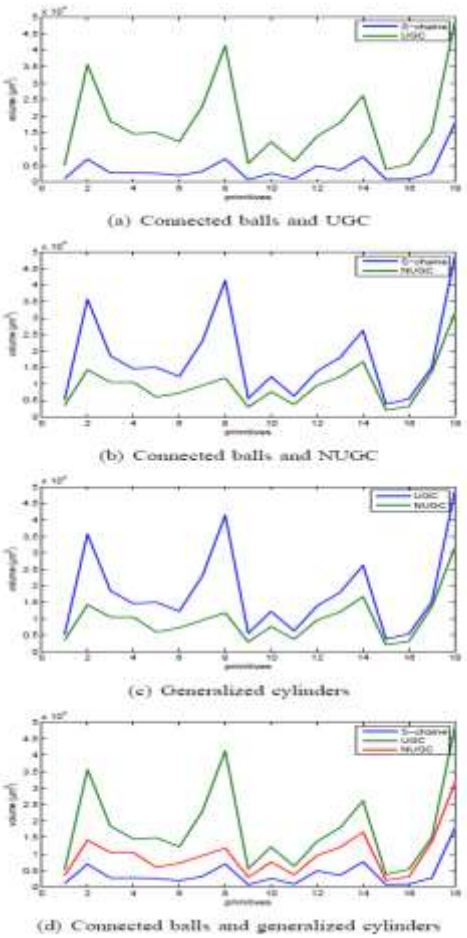

Fig.9 Evolution of the volume computed from the models of pore channel: connected set of balls, uniform generalized cylinder (UGC) and non-uniform generalized cylinder (NUGC)

Fig.9 (c) gives an overview of the evolution of pore channels volume according to the description with simply connected balls chain, uniform generalized cylinder and non-uniform generalized cylinder. Fig.9 (c) shows that the volume decrease according the NUGC, UGC and connected set of balls description. It's also highlight the fact that non uniform generalized cylinders matches more the pore channel shape than the generalized cylinder. From the length and the volume we can easily compute other quantitative characteristics such as tortuosity, porosity and saturated hydraulic conductivity. Other soil water properties such as water content and water saturation can also be easily derived. Thus this representation can be further used for quantitative simulation inside the pore space.

The shape of curves is the same and the volume decrease according to the type of description: NUGC, UGC and connected set of balls. This difference is due to the local quantitative information loss during the approximation process. However, it is worth noting that formula to compute uniform generalized cylinder volume is easier than computing non uniform generalized cylinder.

5.3 Tortuosity

The tortuosity is usually defined as the rapport between the length of the shape skeleton and the distance between the two end points of the skeleton. For connected set of balls representation, Ngom and al. [13] proposed to compute the tortuosity by taking the rapport between the sum of the balls diameter and the distance between the two end points of the connected chain. This proposed method will overestimate the tortuosity because the length of the skeleton is computed as sum of the balls diameters segments. For the generalized cylinders representation, the skeleton is a spline curve and the skeleton length is by construction the generalized cylinder length.
The tortuosity of a generalized cylinder is easily computed easily by using the following equation

$$t = l/d \qquad (20)$$

Where l is the skeleton length given by equation 13 and d the distance between the two end points of the generalized cylinder.

5.4 Satured Hydraulic conductivity

The accurate estimation of hydraulic conductivity is important for many geotechnical engineering applications, as the presence of fluids affects all aspects of soil behavior, including its strength [12]. Saturated hydraulic conductivity is a key indicator to how fast water moves. It is usually estimated using cylindrical column [13,1,26].

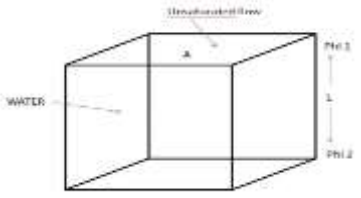

(a) Usual case: cylindrical column

(b) Generalized cylinders as piecewise cylindrical columns

Fig.10 Soil water potential estimation with primitives: the generalized cylinder is subdivided by piecewise cylindrical columns before doing the estimation

1) *Cylindrical based method*: The method is based on a cylindrical column (Fig.10 (a)). In saturated flow, the saturated hydraulic conductivity of water in soil is given by [NGMP11]

$$K_{sat} = \frac{Q}{A}\frac{L}{\varphi_1 - \varphi_2} \qquad (21)$$

Where Q is the volume of water in time t, A is the area of cross section, L is the length of the cylindrical column, φ_1 and φ_2 are water potential at point 1 and at point 2.

2) *Generalized cylinder based method*: We consider a channel approximated by a generalized cylinder that can be uniform or non-uniform. We generalized the usual method on our method, by approximating the generalized cylinders by piecewise cylindrical column. This can be done by straightforward sampling as illustrated by Fig.10(b). In the case of saturated flow, the saturated hydraulic conductivity given by equation 21 becomes

$$K_{sat} = \sum \frac{Q_i}{A_i} * \frac{L_i}{\varphi_{1i} - \varphi_{2i}} \qquad (22)$$

Where Qi is the volume of water in time t, A_i is the area of cross section of the section generalized cylinder, Li length of the section of generalized cylinder, φ_{1i} and φ_{2i} are water potential at point i_1 and at point i_2.

3) *Uniform generalized cylinder based method*: If the channel approximation is performed with uniform generalized cylinders, then it follows from equation 13 that

$$Q_i = S_i l_i = S_i \left\| \frac{5}{12} P_i + \frac{8}{12} P_{i+1} - \frac{1}{12} P_{i+2} \right\|$$

Thus the detailed saturated hydraulic conductivity becomes

$$K_{sat} = \sum \frac{S_i \left\| \frac{5}{12} P_i + \frac{8}{12} P_{i+1} - \frac{1}{12} P_{i+2} \right\|}{A_i} * \frac{L_i}{\varphi_{1i} - \varphi_{2i}} \quad (23)$$

4) *Non uniform generalized cylinder based method*: If the channel approximation is performed with non-uniform generalized cylinders, then it follows from equation 20 that

$$Q_i = \sum_j S_j \left| \left| l_j \right| \right|$$

Where

$$l_j = \frac{5}{12} P_j + \frac{8}{12} P_{j+1} - \frac{1}{12} P_{j+2}$$

Thus, from equation 22, we have

$$K_{sat} = \sum_i \frac{\sum_j S_j \| l_j \|}{A_i} * \frac{L_i}{\varphi_{1i} - \varphi_{2i}} \quad (24)$$

5.5 Porosity

Porosity is the rapport between the volume of pore and the total volume

$$\phi = V_p / V_T \quad (25)$$

Where Vp is the volume of pores and V_T the total volume. If the pores are approximated with

- **uniform generalized cylinder**, then from equation 13 and equation 25, the porosity is given by

$$\phi = \frac{S_i \sum_{i=0}^{n-1} \left\| \frac{5}{12} P_i + \frac{8}{12} P_{i+1} - \frac{1}{12} P_{i+2} \right\|}{V_T} \quad (26)$$

- **non-uniform generalized cylinder**, then from equation 20 and equation 25, the porosity is given by

$$\phi = \frac{\sum_j S_j \| l_j \|}{V_T} \quad (27)$$

Where

$$l_j = \frac{5}{12} P_j + \frac{8}{12} P_{j+1} - \frac{1}{12} P_{j+2}$$

6 Results and Discussion

6.1 Compactness

Approximation with generalized cylinders is straightforward way to gain on compactness of the representation by reduced the number of primitives used to generate the shape. Let us define this number by the degree of compactness.

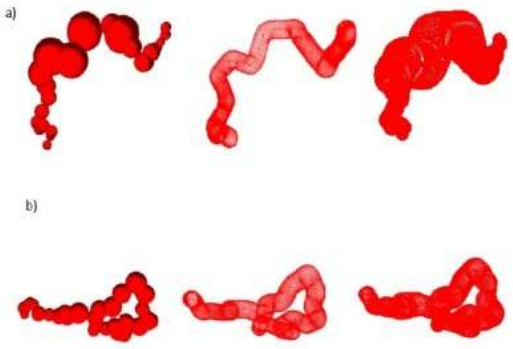

Fig.11 Shape of the generalized cylinders according to the radius of the connected balls set: the variability of the computed shape is 0.2994 for b) and 2.048 for a); the degree of compactness is 26 for b) and 24 for a)

.Fig 11 gives examples where this degree is higher than 20 in the cases of balls representation and 1 in the case of generalized cylinder representation.

6.2 Approximation error

When the radius of balls used to generate the generalized cylinders are not the same, then the uniform generalized cylinder approximation is not suited. As the generalized cylinder is computed from the centers of the balls chain by taking into account the local radius variation, then the standard deviation of the radius of these balls gives a good indication of quality of approximation error. Let $C = \{B_1, \ldots, B_n\}$ a connected set of balls chain and $R = \{r_1, \ldots, r_n\}$ their corresponding radius. The variability of C is defined as the standard deviation of the set of radius R of C.

The variability quantifies the dispersion around the mean of the radius. If all the balls of C have the same radius, then the variability is equal to zero. And more they are differences between the balls radius of C, more the variability is high and more the shape of the computed non-uniform generalized cylinder is different of the shape of the uniform generalized cylinder as illustrated by Figure 10.

- In the first case (Fig.11 a), the mean of the radius is 19.896µm and the variability is 11.065 µm. It is easy to see that the approximation with non-generalized cylinder is better than the approximation with uniform generalized cylinder.
- In the second case, the mean of the radius is 10.7827µm and the variability is 1.6116 µm. The shapes computed from the two approximation procedures are practically the same.

From these observations we can infer that the approximation error is lower for the non-uniform generalized cylinders than for the uniform generalized cylinders. And as a real soil pore galleries have heterogeneous structure, in most cases their variability will be high. Thus for quantitative measures, representation with non-uniform generalized cylinders is more suited.

6.3 Quantitative characteristics

Most pore space quantitative characteristics computation integrated the primitive's length or volume in their equation. As illustrated by the previous section, even if the length is the same for the two types of primitives there are difference in volume between the uniform generalized cylinders and no uniform generalized cylinders owing to the local variability of the later one.

6.4 The processing steps

Our approach is based on an efficient implementation of the approximation process design on an only one platform that can be transformed if needed on net web application. Thus, all the computer code used this work have been written in Java. This enables us to have a more autonomous and dynamic computation processes. We can have different views of the pore space as set of points, balls, uniform generalized cylinders and non-uniform generalized cylinders. Beside, we can also do real time transformations and update the representation very straightforwardly.

7 Conclusion

We proposed a realistic description of soil pore space which can be used to simulate soil functions. This description is an hierarchical representation of pore channel using geometric primitives. We have proposed representation of pore channel with non-uniform generalized cylinders. We showed that these latter matches more real pore system than other primitives by used new concepts such as degree of compactness and variability. These two concepts gives insights on geometrical and topological approximation error. We also provide formulas to compute quantitative characteristics on pore channels or burrow systems such as length, tortuosity, porosity and hydraulic conductivity. We show that all the processes can be done using an only one platform which enables visualization of the pore space as set of points, balls, uniform generalized cylinders and non-uniform generalized cylinders. Illustration and comparative analysis have also been provided.

In the future, we intend to simulate some soil functions (organic matter decomposition, water movement through soil, roots penetration, burrowing activity of earthworms, impacts on the agricultural management) inside the volume computed by the proposed description. Our aim is to build a continuous real time simulation platform computed inside the volume shape extracted after the reconstruction of the pore space of the soil CT images.

Acknowledgment

The authors would like to thank the LTISI laboratory members of the Polytechnic School of This (Dakar, Senegal) for their help, criticism and enthusiasm. They are also grateful to Pr Olivier Monga (IRD, le de France), Pr Patricia Garnier (Inra, Grignon, France), Pr Felix Beckman (Gkss, Research center at Hamburger of HASYLAB, Germany) et Pr Stephan Peth (Institute of Plant Nutrition and Soil Science, Christian Albrechts University of Kiel, Germany) for help in obtaining X-ray images on which the model have been tested.

References

[1] A.S. Ahmed, A. Jardani, A. Revil, and J.P. Dupont. Specific storage and hydraulic conductivity tomography through the joint inversion of hydraulic heads and self-potential data. Advances in water resources, 89:80–90, 2016.

[2] R.S Bartels, J.C Beatly, and B.A Barsky. An introduction to splines for use in computer graphics and geometric modeling. Morgan Kaufmann, 1987.

[3] T. Bultreys, W. De Boever, and V. Cnude. Imaging and image based luid transport modeling at the pore scale in geological materials: a pratical introduction on to the current state of the art. Earth Science Reviews, 155:93–128, 2016.

[4] J.X. Chen and C. Chen. Foundations of 3D graphics programming using JOGL and Java3D. Springer, 2008.
[5] F. Chazal and A. Lieutier. The lambda medial axis. Graphicals Models, 67:304–331, 2005.
[6] M. De Berg, O. Cheong, M.V. Kreveld, and M. Overmars. Computational Geometry: algorithms and applications. Springer, 2008.
[7] S.L. Devadoss and J. ORourKe. Discrete and computational geometry. Princeton university press, 2011.
[8] J. Kress, T.S. Yun, G.A. Narsilio, T.M. Evans, and D.S. Lee. Evaluation of hydraulic conductivity in 3d random and heterogeneous particulate materials using network model. Computers and Geotechnics, pages 45–52, 2012.
[9] O. Monga, P. Garnier, V. Pot, E. Coucheney, N. Nunan, W. Otten, and C. Chenu. Simulating microbial degradation of organic matter in a simple porous system using the 3-d diffusion based model mosaic. Biogeosciences, 11:2201–2209, 2014.
[10] O. Monga, N.F Ngom, and J.F Delerue. Representing geometric structure in 3d tomography soil images : application to pore space modeling. 2007.
[11] F.J. Munoz-ortega, F.S.J. Martinez, and F.J.C. Monreal. Pure applied geophysic, 172:167–179, 2015.
[12] G.A. Narsilio, O. Buzzi, S. Fityus, T.S. Yun, and D.W. Smith. Upscaling of navier stokes equations in porous media: theorical, numerical and experimental approach. Computers and Geotechnics, pages 1200–1206, 2009.
[13] N.F Ngom, P. Garnier, O. Monga, and S. Peth. Modelling three dimensional micro-scale soil structure using a geometrical approach. Geoderma, 163:127–134, 2011.
[14] N.F Ngom, O. Monga, M.O.M Mahmoud, and P. Garnier. 3d shape extraction segmentation and representation of soil microstructures using generalized cylinders. Computer and Geosciences, 39:50–63, 2012.
[15] S.K. Pagenkemper, M. Athmann, D. Uteau, T. Kautz, S. Peth, and R. Horn. The effect of earthworm activity on soil bioporosity investigated with x-ray computed tomography and endoscopy. Soil and tillage Research, 146:79–88, 2015.
[16] S. Peth, R. Horn, F. Beckmann, T. Donath, J. Fischer, and A.J.M. Smucker. Three dimensional quantification of intra aggregate pore space features using synchrotron radiation based microtomography. Soil Science Society of America, 72:897–907, 2008.
[17] V. Pot, S. Peth, O. Monga, L.E. Vogel, A. Genty, P. Gar-
[18] nier, L. Vieubl-Gonod, M. Ogurreck, F. Bekkmann, and P.C.Baveye. Three dimensional distribution of water and air in soil pores: comparison of two phases two relaxation times lattice-boltzmann and morphological model outputs with synchrotron x-ray computed tomography ressources, 84:87–102, 2015.
[19] H. Rogasik, S. Schrader, I. Onasch, J. Kiesel, and H.H. Gerke. Microscale dry bulk density variation around earthworm (lumbricus terrestris l) burrows based on x-ray computed tomography. Geoderma, 213:471–477, 2014.
[20] D. Salomon. Curves and Surfaces for Computer Graphics. Springer, 2006. P.K. Saha, C. Borgefors, and G.S. Di Bija. A survey on skeletonization algorithms and their applications. Pattern Recognition Letters, 76:3–12, 2016.
[21] D. Silin and T. Patzek. Pore space morphology analysis using maximal inscribed spheres. Physica A, 371:336–360, 2006.
[22] L.E. Vogel, D. Makowski, P. Garnier, L. Vieuble-Gonod, Y. Coquet, X. Raynaud, N. Nunan, C. Chenu, R. Falconer, and V. Pot. Advances in Water resources, 83:123–136, 2015.
[23] R. Wieland and H. Rogasik. Computers and Geosciences, 25:96–102, 2015.
[24] D. Wildenschild and A.P. Sheppard. X-ray imaging and analysis techniques for quantifying pore scale structure and processes in subsurface porous medium systems. Advances in water ressources, 51:217–246, 2013.
[25] M. Yashar and M.T. Balhoff. Mesoscale and hybrid models of fluid flow and solute transport. Mineralogical society of america, reviews in mineralogy and geochemistry, 80:433–459, 2015.
[26] S. Zhan, T. Wang, and T. Huang. Variations of hydraulic conductivity of fractur sets and fractured rock mass with test scale: case study at heshe well site in central taiwan. Engineering Geology, 206:94–106, 2016.